AIAA JOURNAL
Vol. 43, No. 9, September 2005

Enthalpy Measurement in Inductively Heated Plasma Generator Flow by Laser Absorption Spectroscopy

Makoto Matsui* and Kimya Komurasaki†
University of Tokyo, Chiba 277-8562, Japan
and
Georg Herdrich‡ and Monika Auweter-Kurtz§
University of Stuttgart, D-70550 Stuttgart, Germany

Laser absorption spectroscopy was applied for diagnostics of inductively heated plasma generator flows. Temporal variation of translational temperature was deduced from measured absorption line broadening because the flow properties fluctuated at 300 Hz in synchronization with the induction current. The specific total enthalpy and mole fraction of oxygen were estimated from the deduced temperature assuming thermochemical equilibrium. Consequently, the averaged degree of dissociation of oxygen is 0.92. The specific total enthalpy was estimated at 33.7 ± 2.9 MJ/kg; 39% of it was in the form of chemical potential. The results show good agreement with intrusive measurements.

I. Introduction

DEVELOPMENT of thermal protection systems (TPS) requires the simulation of entry and reentry conditions at ground-test facilities. Arc heaters are widely used to generate such high-enthalpy flows because of their long operational time, simple structure, and ease of maintenance.[1–4] However, surface catalytic effects and active and passive oxidation of TPS materials have been recognized as important issues[5–8]; erosion of their electrodes poses an important obstacle because polluted flows make it difficult to evaluate chemical reaction rates in front of TPS surfaces.[9,10]

For the reasons just noted, inductively coupled plasma generators have garnered much attention.[11–13] Such generators have no electrode. They can produce an ideal test condition for TPS tests because they have no undesirable chemical reactions that result from erosion. Another advantage of such generators is that they can even use reactive gases such as carbon dioxide and oxygen because of their electrodeless heating. Mars or Venus entry conditions can be simulated using these generators.[14]

An inductively heated plasma generator (IPG3) was developed at the Institut für Raumfahrtsysteme at the University of Stuttgart.[11,14] A schematic of IPG3 and its power supply system is shown in Fig. 1. A Meissner-type resonant circuit is used as an rf oscillator. Its operational frequency can be optimized to achieve high-energy coupling efficiency for various gas species by switching the number of capacitors. Figure 2 shows that the induction current has a specific characteristic. A plasma emission signal measured by a photodetector is also plotted in Fig. 2. Both signals fluctuate at 300 Hz. This fact implies that the flow generated by IPG3 is not stationary.

Various intrusive measurements using a calorimeter, pitot probe, Mach probe, and heat flux probe have been applied to the flows.[15,16] The operational condition and measured parameters by these methods are tabulated in Tables 1 and 2, respectively. Nevertheless, it is still difficult to measure temporal and spatial variations of flow properties, which would be valuable information for validation of intrusive measurements and further studies of TPS surface physics. This study applied laser absorption spectroscopy (LAS) targeting atomic oxygen: the specific enthalpy of the flow was deduced from measurements of line broadening.

II. Measurement Method

In our experimental conditions, Doppler broadening is several gigahertz, which is two orders of magnitude greater than all other broadenings, including natural, pressure, and Stark broadenings. The absorption profile $k(\nu)$ at laser frequency ν is approximated as a Gaussian profile, expressed as[17–20]

$$k(\nu) = (2K/\Delta\nu_D)\sqrt{\ell_n 2/\pi}\exp\left\{-\ell_n 2[2(\nu-\nu_0)/\Delta\nu_D]^2\right\} \quad (1)$$

Here, ν_0 is the center absorption frequency, and K is the integrated absorption coefficient. $\Delta\nu_D$ is the full width at half-maximum of the profile and is related to the translational temperature T expressed as

$$\Delta\nu_D = 2\nu_0\sqrt{\left(2k_BT/mc^2\right)\ell_n 2} \quad (2)$$

where m, c, and k_B are the mass of absorbers, the velocity of light, and the Boltzmann constant, respectively. The number density of absorbers n_i is related to K as

$$n_i = \left(8\pi\nu_0^2/c^2A_{ji}\right)(g_i/g_j)K \quad (3)$$

Here, A_{ji} is the Einstein coefficient, g is the statistical weight, and i, j show absorbing and excited states, respectively. The target line is that of atomic oxygen at 777.19 nm, which is the transition from 3s5S to 3s5P. Because 3s5S is the metastable state, its population is tends to be large in decaying nonequilibrium flows such as supersonic expanding flows.[21]

III. Experimental Apparatus

Figure 3 shows a schematic of the measurement system. A tunable diode laser with an external cavity (Velocity Model 6300, New Focus, Inc.) was used as the laser oscillator. Its linewidth was less than 300 kHz. The laser frequency was scanned over the absorption line shape $k(\nu)$. The modulation frequency and width were 1 Hz and 30 GHz, respectively. The laser intensity I_0, which was normalized by saturation intensity,[20] was 0.08; it was sufficiently small to avoid the influence of absorption saturation.[22] An optical isolator was used to prevent the reflected laser beam from returning into the external

Presented as Paper 2004-1222 at the AIAA 42nd Aerospace Sciences Meeting, Reno, NV, 5–8 January 2004; received 21 October 2004; revision received 16 March 2005; accepted for publication 18 April 2005.

*Graduate Student, Department of Advanced Energy, Kashiwanoha 5-1-5, Kashiwa.
†Associate Professor, Department of Advanced Energy, Kashiwanoha 5-1-5, Kashiwa.
‡Research Engineer, Institut für Raumfahrtsysteme, Pfaffenwaldring 31.
§Professor, Institut für Raumfahrtsysteme, Pfaffenwaldring 31.

Table 1 Operational conditions

Operational condition	Value
Working gas	O_2
Mass flow $\dot{m}$	3 g/s
Anode power P_{anode}	110 kW
Coil turn	5.5
Number of capacitors	4
Chamber ambient pressure p_{amb}	30 Pa

Table 2 Measured parameters[16]

Parameter	Value
Plasma power P_{plasma}	28.2 kW
Total pressure p_0	410 Pa
Mach number M	3
Heat flux density $\dot{q}$	2.1 MW/m^2

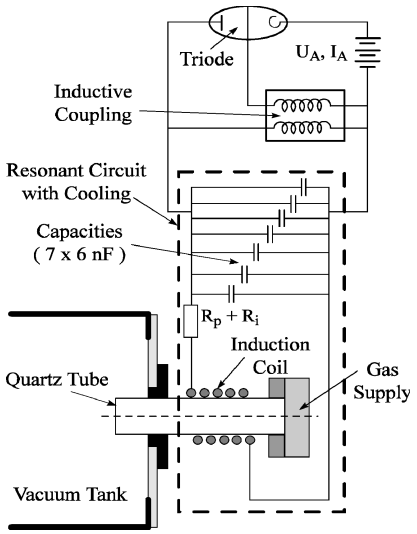

Fig. 1 IPG3 and Meissner-type resonant circuit.

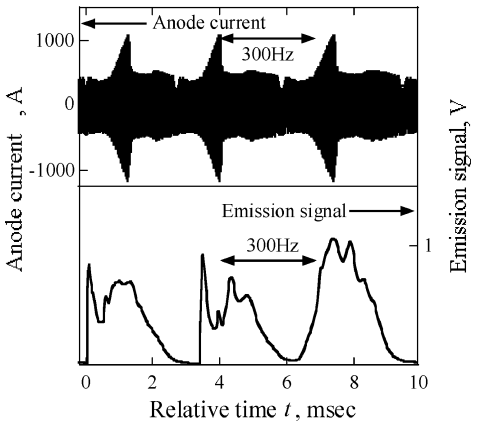

Fig. 2 Induction current and plasma emission signal.

cavity. An etalon was used as a wave meter. Its free spectral range was 1 GHz.

The probe beam was guided to the chamber window through a multimode optical fiber. The fiber output was mounted on a one-dimensional traverse stage to scan the flow in the radial direction. The probe beam diameter was 2 mm at the chamber center. Transmitted laser intensity I was measured at 3 m away from the plume to reduce plasma emission signal by using a photodetector (DET110/M, Thorlabs, Inc.). A parabola mirror allowed scanning of the plume without synchronizing the detector position with the probe beam position. Signals were recorded using a digital oscilloscope (NR-2000, Keyence Co.) with 14-bit resolution at the sampling rate of 20 kHz.

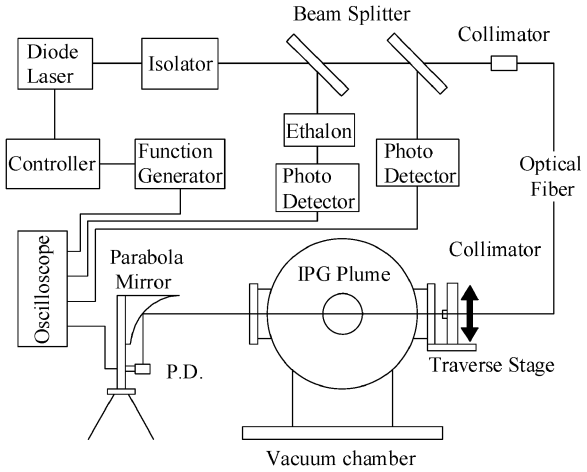

Fig. 3 Measurement system.

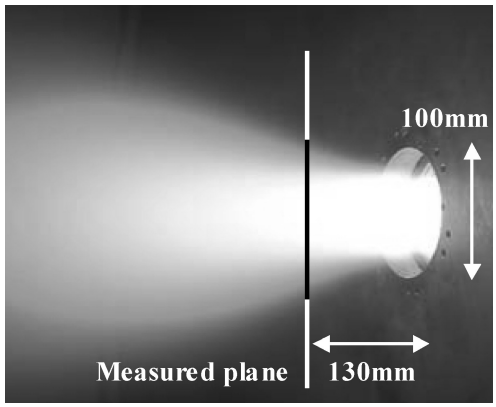

Fig. 4 Photograph of IPG3 plume.

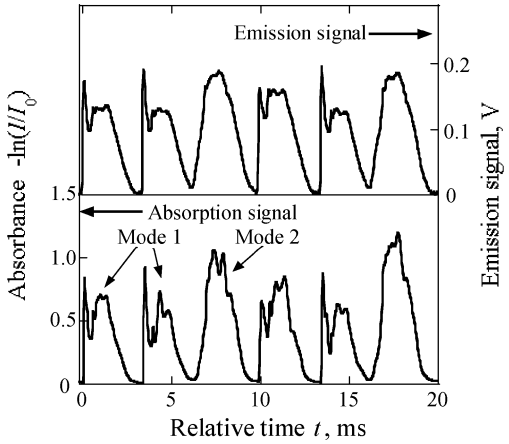

Fig. 5 Absorbance at $\nu = \nu_0 - 4$ GHz and emission signal, $r = 0$ mm.

Figure 4 shows that the measured region was $0 < r < r_{max}$ at 130 mm downstream from the generator exit. Axisymmetric distributions of flow properties were assumed here; r represents the radial coordinate. In this experiment, r_{max} was set at 50 mm, which is equal to the generator exit radius. Table 1 lists operational conditions of the IPG3.

IV. Results

Figure 5 shows the history of an absorbance $-\ln(I/I_0)$ at the fixed laser frequency along with an emission signal. The absorbance fluctuated in synchronization with the emission signal with a period τ of 3.3 ms. The trace is regular and can be categorized into two modes: In mode 1, the trace starts from the zero absorption condition, in which plasma has been extinguished for few hundreds microseconds; in

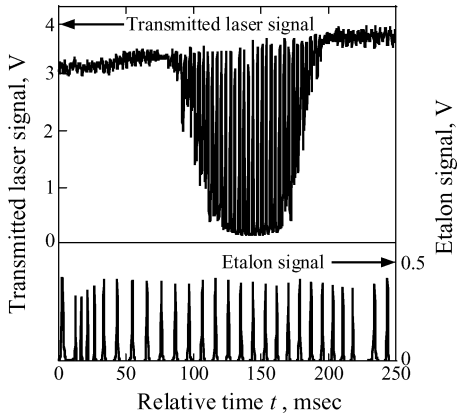

Fig. 6 Typical transmitted laser and etalon signals, $r = 0$ mm.

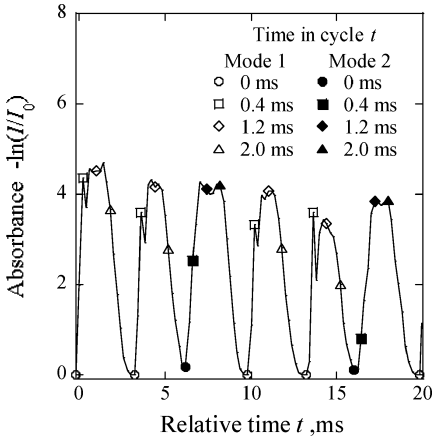

Fig. 7 Typical absorbance and one extraction in each cycle, $r = 0$ mm.

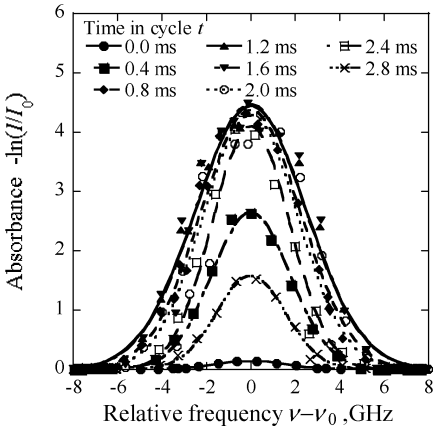

Fig. 8 Temporal variations of path-integrated absorption profile in mode 1, $r = 0$ mm.

mode 2, the trace starts increasing from the nonzero absorption condition, in which plasma is sustained even at the minimum energy input. In this condition, one mode 2 trace regularly appears every three mode traces, as shown in Fig. 5.

Typical signals that were recorded with frequency modulation are shown in Fig. 6 along with an etalon signal. We recorded 40 cycles of frequency modulation for each measurement position. In each cycle, the absorbance is extracted every 0.4 ms. Figure 7 shows typical absorbance that was extracted from the scanned absorption profile. Here, the origin of elapsed time, $t = 0$, is set at the minimum signal in each cycle. Then, we obtained a time-synchronous absorption profile by rearranging the absorbance according to the same elapsed time in the same mode as shown in Fig. 8.

Because the absorbance is composed of path-integrated absorption coefficients, Abel inversion is applied to obtain the absorption

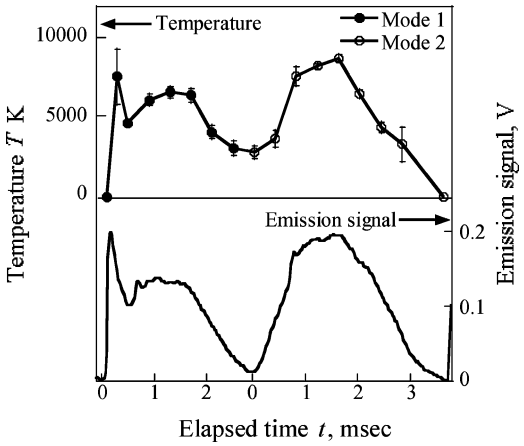

Fig. 9 History of translational temperature and emission signal, $r = 0$ mm.

coefficients. When axisymmetric distributions of flow properties are assumed, the absorption coefficient is obtained by the Abel inversion as

$$k(\nu) = \frac{1}{\pi}\int_r^R \frac{\mathrm{d}\{\ell_n[(I/I_0)(x,\nu)]\}/\mathrm{d}x}{\sqrt{x^2-y^2}}\,\mathrm{d}x \tag{4}$$

Here, x is the distance between the flow axis and the laser path. Because the absorption coefficients are dependent on the frequency, the Abel inversion should be conducted frequency by frequency. Here, after curve fitting to the path-integrated absorption profiles in Fig. 8, the absorbance is extracted every 0.4 GHz from the fitted curves, and then the absorption profile is obtained.

Figure 9 shows that the history of T, as deduced from line broadening of the absorption profiles, was very similar to that of the emission signal. The maximum temperature was 9500 K.

Here, the influence of Doppler shift that originated from the same component with the laser path direction due to the flow expansion as shown in Fig. 4 is estimated. As a result, the temperature on the axis is deduced with less than 5% error because the flow velocity at plume edge is relatively slow.

V. Discussion

A. Temporal Variation of Plasma Properties

The specific total enthalpy h_0 is the sum of static enthalpy

$$\int C_p\,\mathrm{d}T$$

chemical potential h_{chem}, and kinetic energy $u^2/2$ expressed as

$$h_0 = \int C_p\,\mathrm{d}T + h_{\mathrm{chem}} + \frac{1}{2}u^2 \tag{5}$$

Here, C_p is the specific heat at constant pressure, and u is the flow velocity expressed as

$$u = M\sqrt{\gamma RT} \tag{6}$$

Here, γ and R are the specific heat ratio and the gas constant, respectively.

At first thermochemical equilibrium is assumed for simplicity. We estimate h_0 and mole fractions from the measured T and M in Table 2 and calculated $C_p(T)$, $\gamma(T)$, and $R(T)$. In the calculation, three chemical species, O_2, O, and O^+, and two chemical reactions, $O_2 \leftrightarrow 2O$ and $O \leftrightarrow 2O^+ + e^-$, are considered. Their equilibrium constants were obtained from Ref. 23. C_p is computed as the sum of the contributions of each species. Figure 10 shows calculated equilibrium properties at $p_{\mathrm{amb}} = 30$ Pa.

Next, a nonequilibrium effect is considered. In expanding flows, the number density of a metastable state is higher than that from the equilibrium estimation because radiative transitions to lower states

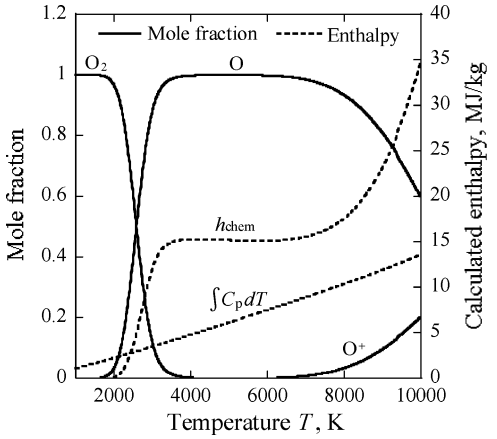

Fig. 10 Calculated enthalpy and mole fractions by thermochemical equilibrium assumptions, $p_{amb} = 30$ Pa.

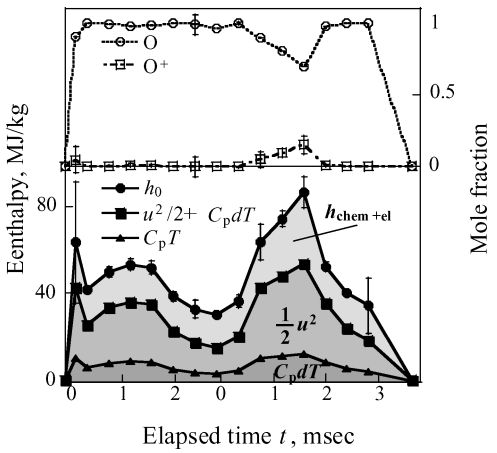

Fig. 11 History of estimated enthalpy and mole fractions, $r = 0$ mm.

are forbidden. This additional electronic excitation enthalpy h_{el} can be estimated using measured metastable population density n_i as

$$h_{el} = n_i E_i / \rho \tag{7}$$

Here, E_i is the excitation energy of the metastable state, and ρ is the density defined as $\rho = p_{amb}/k_B T$. However, the following results might still underestimate actual flow enthalpy because the nonequilibrium ionization effect could not be estimated here.

Figure 11 shows the history of estimated properties on the plume axis. Maximum h_0 was 86 MJ/kg, and at that time, the mole fraction of atomic oxygen was 0.7 because of ionization. The averaged degree of dissociation of oxygen is 0.92.

B. Time-Averaged Specific Total Enthalpy

The time-averaged specific total enthalpy $\bar{h}_0(r)$ is defined as

$$\bar{h}_0(r) = \frac{\int_0^\tau h_0(r,t)\rho(r,t)u(r,t)\,\mathrm{d}t}{\int_0^\tau \rho(r,t)u(r,t)\,\mathrm{d}t} \tag{8}$$

Figure 12 shows the distribution of $\bar{h}_0(r)$ estimated from the measured and calculated parameters. Although it took a maximum of 33.7 ± 2.9 MJ/kg on the axis, the profile was almost flat for the TPS probe area, $r < 10.5$ mm. Figure 13 shows the enthalpy balance at $r = 0$, where $\bar{h}_{chem}$ accounted for 38.7% of $\bar{h}_0$.

C. Comparison with Intrusive Measurements

Plasma power $P_{plasma,\, r<r\,max}$ and the mass flow rate $\dot{m}_{r<r\,max}$ contained in the measured cylinder of the flow are obtained as

$$P_{plasma, r<r_{max}} = \int_0^{r_{max}} 2\pi r \rho(r) u(r) \bar{h}_0(r)\,\mathrm{d}r \tag{9}$$

Table 3 Comparison of P_{plasma}

Method	r_{max}, mm	P_{plasma}, kW	$\dot{m}_{r<r\,max}$, g/s
LAS (present)	50	17.5	0.86
Calorimeter[22]	60	28.2	3 (assumed)

Table 4 Comparison of $\bar{h}_0$ (0)

Method	$\bar{h}_0$ (0), MJ/kg
LAS (present)	33.7 ± 2.9
Intrusive measurements[16]	30.5

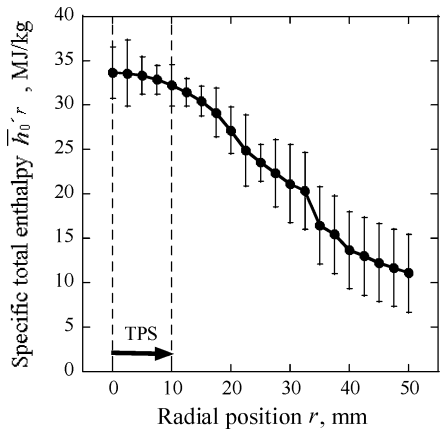

Fig. 12 Time-averaged specific total enthalpy distribution.

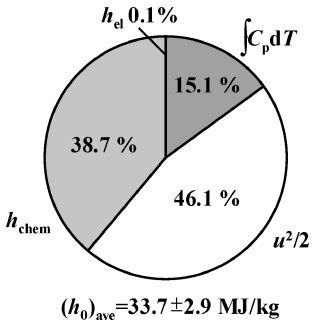

Fig. 13 Enthalpy balance, $r = 0$ mm.

$$\dot{m}_{r<r_{max}} = \int_0^{r_{max}} 2\pi r \rho(r) u(r)\,\mathrm{d}r \tag{10}$$

Table 3 shows those results in comparison with the calorimeter measurements. Figure 4 shows that $P_{plasma,\, r<r\,max}$ in LAS is smaller than those of calorimeter measurements[16] because the flow has expanded to the region of $r > r_{max}$.

In Ref. 16, $\bar{h}_0(r)$ was estimated from the measured $\dot{q}(r)$, $p_0(r)$, and P_{plasma} by using Pope's relation (see Ref. 24) as

$$\bar{h}_0(r) = \frac{r_{max}^2}{2} \frac{\dot{q}(r)\Big/\sqrt{p_0(r)}}{\int_0^{r_{max}} \left[\dot{q}(r)\Big/\sqrt{p_0(r)}\right] r\,\mathrm{d}r} \frac{P_{plasma,\, r<r_{max}}}{\dot{m}_{r<r_{max}}} \tag{11}$$

Here, $\dot{m}_{r<r\,max} = \dot{m} = 3$ g/s was assumed regardless of $r_{max} = 60$ mm. Table 4 shows a comparison between intrusive measurements[16] and present study. Results show good agreement. The values would more closely resemble one another than those in Table 3 if $\dot{m}_{r<r\,max}$ is estimated precisely in intrusive measurements.

VI. Summary

LAS was applied for the diagnostics of nonstationary IPG3 flow. Consequently, the averaged degree of dissociation of oxygen is 0.92. The total enthalpy was estimated as 33.7 ± 2.9 MJ/kg; 39% of it

was possessed as the chemical potential. These results show good agreement with intrusive measurements.

References

[1]Birkan, M. A., "Arcjets and Arc Heaters: An Overview of Research Status and Needs," *Journal of Propulsion and Power*, Vol. 12, No. 6, 1996, pp. 1011–1017.

[2]Milos, F. S., "Flowfield Analysis for High-Enthalpy Arc Heaters," *Journal of Thermophysics and Heat Transfer*, Vol. 6, No. 3, 1992, pp. 565–568.

[3]Auweter-Kurtz, M., Kurtz, H. L., and Laure, S., " Plasma Generators for Reentry Simulation," *Journal of Propulsion and Power*, Vol. 12, No. 6, 1996, pp. 1053–1061.

[4]Lago, V., Lebéhot, A., Dudeck, M., Pellerin, S., Renault, T., and Echegut, P., "Entry Conditions in Planetary Atmospheres: Emission Spectroscopy of Molecular Plasma Arcjets," *Journal of Thermophysics and Heat Transfer*, Vol. 15, No. 2, 2001, pp. 168–175.

[5]Curry, D. M., Pham, V. T., Norman, I., and Chao, D. C., "Oxidation of Hypervelocity Impacted Reinforced Carbon," *Journal of Spacecraft and Rockets*, Vol. 37, No. 2, 2000, pp. 310–317.

[6]Goulard, R., "On Catalytic Recombination Rates in Hypersonic Stagnation Heat Transfer," *Jet Propulsion*, Vol. 28, No. 11, 1958, pp. 737–745.

[7]Balat, M., and Berjoan, R., "Oxidation of Sintered Silicon Carbide under Microwave-Induced CO_2 Plasma at High Temperature: Active–Passive Transition," *Journal of Applied Surface Science*, Vol. 161, Nos. 3–4, 2000, pp. 434–442.

[8]Bykova, N. G., Vasil'evskii, S. A., Gordeev, A. N., Kolesnikov, A. F., Pershin, I. S., and Yakushin, M. I., "Determination of the Effective Probabilities of Catalytic Reactions on the Surfaces on Heat Shield Materials in Dissociated Carbon Dioxide Flows," *Journal of Fluid Dynamics*, Vol. 32, No. 6, 1997, pp. 876–886.

[9]Milos, F. S., and Shepard, C. E., "Thermal Analysis of an Arc-Heater Electrode with a Rotating Arc Foot," *Journal of Thermophysics and Heat Transfer*, Vol. 8, No. 4, 1994, pp. 723–729.

[10]Durgapal, P., "Electrode Phenomena in High-current, High-Pressure Arc Heaters," *Journal of Thermophysics and Heat Transfer*, Vol. 7, No. 3, 1993, pp. 412–417.

[11]Herdrich, G., Auweter-Kurtz, M., and Kurtz, H., "New Inductively Heated Plasma Source for Reentry Simulations," *Journal of Thermophysics and Heat Transfer*, Vol. 14, No. 2, 2000, pp. 244–249.

[12]Bottin, B., Varbonaro, M., Van der Haegen, V., and Paris, S., "Predicted and Measured Capability of the VKI 1.2MW Plasmatron Regarding Re-Entry Simulation," 3rd European Symposium on Aerothermodynamics for Space Vehicles, ESA SP-426, 1998, pp. 553–560.

[13]Gordeev, A. N., "Overview of Characteristics and Experiments in IPM Plasmatrons," *Measurement Techniques for High Enthalpy and Plasma Flows, NATO Research and Technology Organization Proceedings*, RTO EN-8, 2000, pp. 1A-1–1A-18.

[14]Herdrich, G., Auweter-Kurtz, M., Endlich, P., and Kurtz, H., "Mars Entry Simulation Using an Inductively Heated Plasma Generator," *Journal of Propulsion and Power*, Vol. 40, No. 5, 2003, pp. 690–693.

[15]Herdrich, G., Auweter-Kurtz, M., Kurtz, H., Laux, T., and Winter, M., "Operational Behavior of Inductively Heated Plasma Source IPG3 for Entry Simulations," *Journal of Thermophysics and Heat Transfer*, Vol. 16, No. 3, 2002, pp. 440–449.

[16]Herdrich, G., and Auweter-Kurtz, M., "Development and Characterization of Inductively Heated Plasma Generator for Atmospheric Entry Simulations," AIAA Paper 2004-2503, June 2004.

[17]Baer, D. S., Nagali, V., Furlong, E., Hanson, R. K., and Newfield, M. E, "Scanned- and Fixed-Wavelength Absorption Diagnostics for Combustion Measurements Using Multiplexed Diode Lasers," *AIAA Journal*, Vol. 34, No. 3, 1996, pp. 489–493.

[18]Hanson, R. K., "Absorption Spectroscopy in Sooting Flames Using a Tunable Diode Laser," *Applied Optics*, Vol. 19, No. 4, 1980, pp. 482–484.

[19]Matsui, M., Takayanagi, H., Oda, Y., Komurasaki, K., and Arakawa, Y., "Performance of Arcjet-Type Atomic-Oxygen Generator by Laser Absorption Spectroscopy and CFD Analysis," *Vacuum*, Vol. 73, No. 3, 2004, pp. 341–346.

[20]Yariv, A., *Quantum Electronics*, 2nd ed., Wiley, New York, 1975, Chap. 8.

[21]Park, C., *Nonequilibrium Hypersonic Aerothermodynamics*, Wiley, New York, 1990, pp. 89–97.

[22]Matsui, M., Ogawa, S., Komurasaki, K., and Arakawa, Y., "Absorption Saturation in Laser Absorption Diagnostics," *Journal of Institute of Applied Plasma Physics*, Vol. 10, 2002, pp. 17–22 (in Japanese); also *Applied Optics* (submitted for publication).

[23]Guputa, R. N., Yos, J. M., Thompson, R. A., and Lee, K.-P., "A Review of Reaction Rates and Thermodynamic and Transport Properties for an 11-Species Air Model for Chemical and Thermal Nonequilibrium Calculations to 30000 K," NASA RP-1232; L-16634; NAS 1.61:1232, 19900801, Aug. 1990.

[24]Marvin, J. G., and Pope, R.B., "Laminar Convective Heating and Ablation in the Mars Atmosphere," *AIAA Journal*, Vol. 5, No. 2, 1967, pp. 240–248.

R. Lucht
Associate Editor